



RESEARCH LETTER

10.1029/2021GL097157

Key Points:

- The model spread in tropical cyclone frequency is modulated by the precursory vortex seed frequency
- The seed frequency is related to the large-scale circulation via the seed propensity index
- The model spread is larger in response to uniform sea surface temperature (SST) increase than to El Niño-Southern Oscillation-like SST perturbations

Correspondence to:

T.-L. Hsieh,
hsiehl@princeton.edu

Citation:

Hsieh, T.-L., Yang, W., Vecchi, G. A., & Zhao, M. (2022). Model spread in the tropical cyclone frequency and seed propensity index across global warming and ENSO-like perturbations. *Geophysical Research Letters*, 49, e2021GL097157. <https://doi.org/10.1029/2021GL097157>

Received 29 NOV 2021
Accepted 12 MAR 2022

Model Spread in the Tropical Cyclone Frequency and Seed Propensity Index Across Global Warming and ENSO-Like Perturbations

Tsung-Lin Hsieh¹ , Wenchang Yang² , Gabriel A. Vecchi^{1,2} , and Ming Zhao³

¹High Meadows Environmental Institute, Princeton University, Princeton, NJ, USA, ²Department of Geosciences, Princeton University, Princeton, NJ, USA, ³National Oceanic and Atmospheric Administration, Geophysical Fluid Dynamics Laboratory, Princeton, NJ, USA

Abstract The future projection of tropical cyclone frequency is highly uncertain. Recent multi-model studies showed that the model spread in tropical cyclones is correlated with the model spread in seeds, which are defined as convective weak vortices. However, it was unclear how the model spread is related to the large-scale circulation. Here we apply a downscaling theory recently developed using aquaplanet experiments to explain the seed frequency across four global atmospheric models having different parameterizations of convection and resolutions. The seed frequency has a larger model spread in response to uniform warming than to CO₂ doubling or El Niño/La Niña-like sea surface temperature perturbations. Across all climate perturbations, the seed frequency is captured by the downscaling theory, expressed as a seed propensity index. The index highlights the connection between the tropical cyclone seeds and the climatological mean ascent pattern.

Plain Language Summary Climate models provide reliable projections on the change of rain rate when averaged over the entire tropics. The regional change of tropical cyclones (TCs) and their precursors is less certain. Climate change simulations show that the number of TCs per year is strongly influenced by the number of raining and rotating disturbances (seeds) that precede the development of TCs. The number of seeds is related to the large-scale circulation, quantified by a recently developed index. When this index increases, the model generates more seeds, and in the more climatically plausible conditions more TCs; when this index decreases, the model is likely to generate fewer seeds and TCs.

1. Introduction

Tropical cyclones (TCs) are some of the most dangerous natural hazards. Understanding how their frequency changes with climate has a significant socioeconomic impact. Statistical correlations between the observed TC frequency and the surrounding environment have been developed since the 1970's (Gray, 1979), but the correlations are complex and the extrapolation to future conditions is not constrained by historical records (Camargo et al., 2014; Emanuel, 2020).

To capture the full complexity of the changing environmental conditions, high-resolution coupled global climate models (GCMs) are widely used to simulate the global circulation and TCs in a consistent framework. In simulations of radiatively forced climate change, the response of TC frequency has a large spread among coupled GCMs. A recent multi-model comparison by Knutson et al. (2020) showed that the response is between an increase of 22% and a decrease of 28% per 2 K of mean surface temperature increase. The uncertainty in the sign of TC frequency response is also seen in different methods combining statistical and dynamical downscaling models of TCs (Emanuel, 2020; Jing et al., 2021; Lee et al., 2020), which further illustrates the difficulty of constraining future TC frequency using existing observations and theory.

Recently, a seeding-transition framework has been developed to explain the TC variation across climate perturbations (Hsieh, Vecchi, et al., 2020; Vecchi et al., 2019) and the annual cycle (Yang et al., 2021). In this framework, the TC evolution is decomposed into two stages, including a seeding stage followed by a transition stage. In the seeding stage, a convective weak vortex, referred to as a seed, is generated within the large-scale circulation. The frequency of seeds has been found to have a significant impact on the frequency of TCs in response to climate change in several models (Sugi et al., 2020; Vidale et al., 2021; Yamada et al., 2021).

© 2022. The Authors.

This is an open access article under the terms of the [Creative Commons Attribution License](https://creativecommons.org/licenses/by/4.0/), which permits use, distribution and reproduction in any medium, provided the original work is properly cited.

In the transition stage, a seed evolves into a TC with a probability that depends on the ventilation index, which is a function of the environmental potential intensity, saturation deficit, and vertical wind shear (Hoogewind et al., 2020; Hsieh, Vecchi, et al., 2020; Tang & Camargo, 2014; Vecchi et al., 2019; Yang et al., 2021). The transition probability is less important to explain the response of TC frequency to climate change (Hsieh, Vecchi, et al., 2020), but it is important to explain the response to the annual cycle (Yang et al., 2021) and to the interannual variability (Ikehata & Satoh, 2021).

While a significant source of the uncertainty in TC projections has been identified to be the uncertainty in the seed frequency (Yamada et al., 2021), it is not clear how the latter is related to the model spread in the large-scale circulation. In this study, we apply a downscaling theory for seeds developed based on dynamical scale analysis and aqua planet experiments (Hsieh, Vecchi, et al., 2020) to multiple models that show opposite changes of seeds. A large number of experiments are performed using four atmospheric models with different parameterizations of convection and resolutions. This study complements the single model results in Hsieh, Vecchi, et al. (2020) and the annual cycle results in Yang et al. (2021), and shows that the downscaling theory explains the seed frequency across models.

2. Methods

2.1. Models

We utilize four global atmospheric models developed at the Geophysical Fluid Dynamics Laboratory (GFDL) that have been applied extensively in TC research. The models are HiRAM-50km, AM2.5-50km, AM2.5-25km, and AM4-50km. The HiRAM model, having a horizontal grid spacing of 50 km, has been shown to capture the global (Zhao et al., 2009) and regional TC activity across seasonal (Zhao & Held, 2010) to interannual (Chen & Lin, 2011) time scales.

The AM2.5-50km model is the atmospheric component of the coupled model Forecast-oriented Low Ocean Resolution (FLOR) (Vecchi et al., 2014) and has the same horizontal resolution as HiRAM. The AM2.5-25km model is the atmospheric component of the coupled model HiFLOR (Murakami et al., 2015), having a smaller horizontal grid spacing of 25 km. The FLOR model is skillful in the seasonal TC forecast (Vecchi et al., 2014). The HiFLOR model inherits many properties of FLOR and additionally captures the frequency of major hurricanes (Murakami et al., 2015). Notably, the TC response in HiFLOR is on the high end of the multi-GCM spread (Bhatia et al., 2018).

The AM4 model is the latest generation of atmospheric model developed at GFDL, which has been used in Model Intercomparison Projects including CMIP6 and HighResMIP (Zhao, 2020). It is capable of capturing the observed annual cycle and geographical distribution of TC frequency with a horizontal grid spacing of 100 km (Zhao et al., 2018). Here we use a higher resolution version of 50 km, which better simulates the synoptic-scale atmospheric variability (Zhao, 2020).

The models have the same dynamical core and are closely related to each other, but they have different representations of unresolved processes, in particular the convective parameterization schemes. While all models we use are skillful in capturing the observed TC activity given sea surface temperature (SST), they cover a wide range of TC responses to future warming climates, similar to the spread of coupled GCMs (Knutson et al., 2020).

2.2. Experiments

A large number of experiments are performed and summarized in Table 1. To control for internal climate variability and to isolate the atmospheric response to SST, we prescribe identical SST and radiative forcing to our models. For the first three models (HiRAM-50km, AM2.5-50km, and AM2.5-25km), the control experiment is driven by the annual cycle of SST averaged between 1986 and 2005 following Vecchi et al. (2019). The annual cycle is repeated 40 times after 10 years of model spin up, so that the 40 year mean represents the climatological annual cycle.

Similar to Held and Zhao (2011), experiments with uniform 2 K warming, CO₂ doubling, and combined perturbations are performed. The SST perturbation for the RCP4.5 late 21st century warming experiment is constructed using the mean response of 17 models in the Coupled Model Intercomparison Project Phase 5 following

Table 1
List of Experiments and Reanalysis Used in This Study

Time slice experiments			
Model	HiRAM-50km AM2.5-25km AM2.5-50km		AM4-50km
Analysis period	40 years		20 years
Experiment	Control +2 K $2 \times \text{CO}_2$ +2 K & $2 \times \text{CO}_2$ RCP4.5 El Niño La Niña Warming SST > 28C Warming SST < 28C		Control +4 K $4 \times \text{CO}_2$
Time series experiments/reanalysis (1980–2015)			
Model	HiRAM-50km AM2.5-50km	AM2.5-25km	ERA5 reanalysis (Hersbach et al., 2020)
Ensemble size	5	3	1
<i>Note.</i> The time slice experiments are used to generate Figure 1 and Figures 2a and 2b. The time series experiments/reanalysis are used to generate Figure 2c.			

van der Wiel et al. (2017) and Bhatia et al. (2018). In addition, experiments with extreme perturbations of the SST gradient are performed following Hsieh, Vecchi, et al. (2020). To briefly summarize, the “warming SST > 28C” experiment increases the SST warmer than 28°C by 1 K; while “warming SST < 28C” experiment increases the SST cooler than 28°C by 1 K.

Two additional experiments are designed for this study: the El Niño and La Niña experiments. The SST annual cycles are averaged over the nine strongest El Niño years between 1980 and 2015 whose Oceanic Niño Indices are greater than 1: 1982, 1986, 1987, 1991, 1994, 1997, 2002, 2009, 2015. Similarly, the SST annual cycles are averaged over the seven strongest La Niña years in this time frame whose Oceanic Niño Indices are less than -1: 1988, 1995, 1998, 1999, 2007, 2010, 2011. The CO₂ concentration is the same in all experiments, except in the CO₂ doubling experiment.

The AM4-50km experiments have a slightly different control climate, whose SST annual cycle is averaged between 1980 and 2014 (Zhao, 2020). The control, uniform 4 K warming, and CO₂ quadrupling experiments are performed over 30 repeating annual cycles, and the last 20 years are analyzed. The experiments have been used to study atmospheric rivers (Zhao, 2020).

Lastly, historical experiments are performed with SST time series from the Atmospheric Model Intercomparison Project (Durack & Taylor, 2018). An ensemble of five simulations are performed for HIRAM-50km and AM2.5-50km. The ensemble size is 3 for the more expensive AM2.5-25km. The ensembles are constructed by perturbing the initial conditions following Yang et al. (2021).

2.3. Identification Algorithms for TCs and Seeds

TCs are tracked using an algorithm that includes criteria on sea-level pressure local minimum, surface wind speed, warm core, and lifetime (Harris et al., 2016). The threshold values for the models we use follow Yang et al. (2021) and are calibrated against observations. The values influence the absolute number of TCs but have little influence on the percentage change from the control climate.

Seeds are tracked using an algorithm based on the six-hourly snapshots of precipitation rate and 850 hPa vorticity fields (Hsieh, 2022). Seeds are defined as clusters of extreme precipitation (>99.5th percentile of instantaneous precipitation rates between 30°S and 30°N) with diameter greater than 100 km, whose 850 hPa relative vorticity at any instance over the lifetime exceeds $4 \times 10^{-4} \text{ s}^{-1}$. Clusters between two consecutive snapshots are connected if their centroids are no more than 300 km apart, meaning that the average translation speed over the six hour time span is less than 50 km hr^{-1} . The tracker parameters are determined in Hsieh, Vecchi, et al. (2020), such that the lowest vorticity seed corresponds to when the sea-level pressure minimum occurs. The same thresholds are used for the three 50 km models (HiRAM-50km, AM2.5-50km, and AM4-50km). The number of seeds is approximately three times the number of TCs in the control climate.

For the higher-resolution model, AM2.5-25km, the model output is interpolated to the 50 km grid before applying the same seed tracker with some modifications of thresholds. Because it better resolves the vortex core, the vorticity threshold is increased by a factor of 2. In addition, because low resolution models tend to overestimate the extreme precipitation rate compared with high resolution models, even after interpolating to the same grid (Hsieh, Garner, & Held, 2020), the percentile precipitation rate threshold is reduced from 99.5th to 99th, such that seeds in the 25 km and 50 km models have similar size distributions and total rainfall. Analogous to the TC tracker thresholds, the seed tracker thresholds influence the absolute number of seeds but have little influence on the percentage change from the control to the perturbed climate.

2.4. The Climatological Seed Propensity Index

The seed propensity index (SPI) is designed to parameterize the propensity for seeds to occur within the large-scale circulation. SPI is defined as:

$$S = -\omega \frac{1}{1 + Z^{-1/\alpha}}, \quad (1)$$

$$\text{where } Z = \frac{f + \zeta}{\sqrt{|\beta + \partial_y \zeta| U}}. \quad (2)$$

The monthly mean vertical velocity averaged over 40 years (or 20 years for AM4-50km) on the pressure coordinate, ω , is evaluated at 500 hPa. The descending portion of ω is zeroed out.

In the non-dimensional parameter Z , f and β represent the Coriolis parameter and its meridional gradient, ζ is the monthly mean relative vorticity at 850 hPa, and $U = 20 \text{ m s}^{-1}$ and $\alpha = 0.69$ are fitting parameters determined in aquaplanet simulations (Hsieh, Vecchi, et al., 2020). The numerator, which is the absolute vorticity, is replaced with zero if it is negative (i.e., anticyclonic).

The fraction $1/(1 + Z^{-1/\alpha})$ scales as $Z^{1/\alpha}$ near the equator, but it is close to a linear dependence on Z within 10% (Hsieh, Vecchi, et al., 2020). The percentage change of SPI with climate is fairly insensitive to the fitting parameters, as long as this fraction increases from zero near the equator and approaches a constant in the subtropics.

The non-dimensional parameter Z represents the ratio between the vortex stretching term and the advection of planetary vorticity term in the low-level vorticity equation, which is a proxy for the rate of vorticity increase for a developing tropical disturbance (Hsieh, Vecchi, et al., 2020).

2.5. The Climatological Ventilation Index and Transition Probability

The probability that a seed transitions into a TC is parameterized by a sigmoid function of the ventilation index:

$$p = \frac{1}{1 + (\Lambda_0/\Lambda)^{-1/\gamma}}, \quad (3)$$

$$\text{where } \Lambda = \frac{v_s \cdot \mathcal{X}}{v_p}. \quad (4)$$

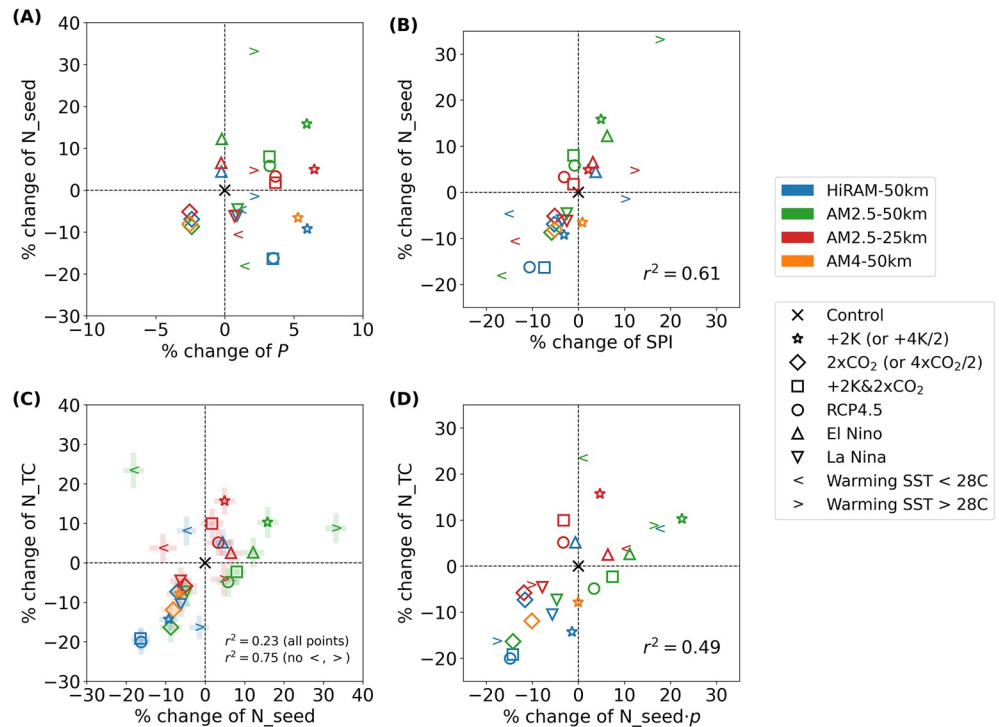


Figure 1. Relationships between the frequency of tropical cyclones (TCs), seeds, and the climate state. (a) The simulated seed frequency versus the tropical mean precipitation (P). (b) The simulated seed frequency versus the tropical mean seed propensity index (SPI). (c) The simulated TC frequency versus the simulated seed frequency; $r^2 = 0.23$ for all experiments and $r^2 = 0.75$ excluding the warming 28C experiments. The lightly shaded bars indicate the 95% confidence intervals calculated from the interannual time series. (d) The simulated TC frequency versus the simulated seed frequency multiplied by the ventilation-based probability (p). All quantities are integrated over the tropics (30°S – 30°N) before computing the percentage change relative to the control experiment. The colors indicate the models, and the symbols indicate the climate perturbations.

The non-dimensional ventilation index Λ is computed using the monthly mean vertical wind shear v_s multiplied by the non-dimensional saturation deficit χ and divided by the potential intensity v_p calculated based on the monthly mean thermodynamic profiles (Bister & Emanuel, 2002). The typical ventilation index $\Lambda_0 = 0.014$ and the fitting parameter $\gamma = 0.89$ have been determined observationally (Tang & Emanuel, 2012) and used to explain the annual cycle of TCs in global atmospheric models (Yang et al., 2021).

When computing the global mean, SPI is averaged over all oceans within 30°S – 30°N as it indicates the location of seed formation. On the other hand, the probability p is averaged over subtropical oceans (30° – 10°S and 10° – 30°N) having SST warmer than 26°C , representing the mean environment encountered by the entire seed trajectories.

3. Results

3.1. The Global Response of Seeds

To understand the model response to the diverse climate perturbations, we first compare the change of tropical mean precipitation and show that it is consistent across models. We then show that this quantity does not constrain the model spread in seed frequency, and that the SPI is a more relevant large-scale quantity. The model spread in seed frequency is then compared with the model spread in TC frequency.

Figure 1a compares the seed frequency with the tropical mean precipitation across all time slice experiments and models. In response to CO_2 doubling and unchanged SST, the seed frequency decreases in every model. This is consistent with the decrease of tropical mean precipitation, combined with qualitatively similar atmospheric

circulation responses across models. On the other hand, the circulation responses (quantified in the following by SPI) are different with respect to uniform 2 K warming, leading to opposite signs of seed frequency changes. While the change of mean precipitation with surface temperature increase is constrained by theory (Jeevanjee & Romps, 2018) and consistent across models (the same symbols line up vertically in Figure 1a), it does not constrain the sign of the seed response.

It is necessary to consider the spatial pattern of the large-scale ascent and the absolute vorticity, quantified by SPI (Equation 1). In SPI, the climatological vertical velocity ω is balanced with the energy flux convergence into the atmospheric column divided by the gross moist stability (Hsieh, Vecchi, et al., 2020), suggesting that it represents the ascending motion associated with large-scale energy balance, rather than small-scale convective dynamics.

The other factor in SPI, which is a sigmoid function of Z , gives larger weights to the off-equatorial ω , as larger background vorticity favors the formation of seeds due to vortex stretching. SPI captures the response of explicitly simulated vortex seeds with $r^2 = 0.61$ (Figure 1b). In comparison, the tropical mean precipitation fails to capture the different signs of responses to +2 K across models (the star symbols in Figure 1a).

We include the AM4–50km model to stress test SPI. The model is driven by stronger climate perturbations, including uniform surface warming of 4 K and quadrupling of CO_2 concentration. In Figure 1, the +4 K and $4 \times \text{CO}_2$ responses are divided by two to compare with the +2 K and $2 \times \text{CO}_2$ responses in the other models. The AM4–50km results are in between the HiRAM–50km and the two AM2.5 models. They follow the same linear relationship in Figure 1b, providing further evidences for the generality of SPI.

The response of TC frequency is compared with the response of seed frequency in Figure 1c. Seeds are convective weak vortices, which have approximately 40% of the minimum TC vorticity. The transition probability from seeds to TCs vary between 25% and 60% depending on the experiment. The “warming SST > 28C” experiment is designed to enhance the tropical SST gradient, increasing the ventilation index and decreasing the transition probability; and vice versa for the “warming SST < 28C” experiment. Therefore, the responses of seeds and TCs are more distinct with these two perturbations.

The difference between the responses of seed frequency and TC frequency for the two warming 28C perturbations is reduced when the seed frequency is multiplied by the ventilation-based probability, p (Equation 3). The correlation is $r^2 = 0.49$ across all perturbations in Figure 1d, higher than $r^2 = 0.23$ in Figure 1c. The improved correlation by including p is consistent with the findings of Hsieh, Vecchi, et al. (2020) for a single model and Yang et al. (2021) for the TC annual cycle.

When the two warming 28C perturbations are excluded, the correlation between seeds and TCs increases from $r^2 = 0.23$ to $r^2 = 0.75$ with a slope close to 1 in Figure 1c. That is, the transition probability changes modestly in response to the more climatically plausible perturbations.

Consistent with findings from models developed at other institutions (Walsh et al., 2015), the TC frequency response to +2 K has a larger model spread than to $2 \times \text{CO}_2$. This difference is captured by the model spread in the seed frequency.

3.2. The Basin-Scale Response of Seeds

Since SPI incorporates the spatial structures of the climatological vertical velocity and absolute vorticity, it is able to capture the geographical variability of seeds. Figure 2 shows the spatial integral of SPI (bars) and the simulated seed frequency (circles) over major ocean basins. Note that the basin-wide percentage change is calculated relative to the global sum rather than the basin sum, so this value summed over all basins is the global percentage change.

Across all panels in Figure 2, the model spread is dominated by the North Pacific, consistent with results from the High Resolution Model Intercomparison Project (Roberts et al., 2020). The North Pacific is separated into three sub-basins to emphasize the model spread over the warm pool region. The boundary between the Northwest and Northcentral Pacific is at 145° longitude to separate the warm pool and the cold tongue. The boundary between the Northcentral and Northeast Pacific is at 205° longitude so that they have approximately equal area.

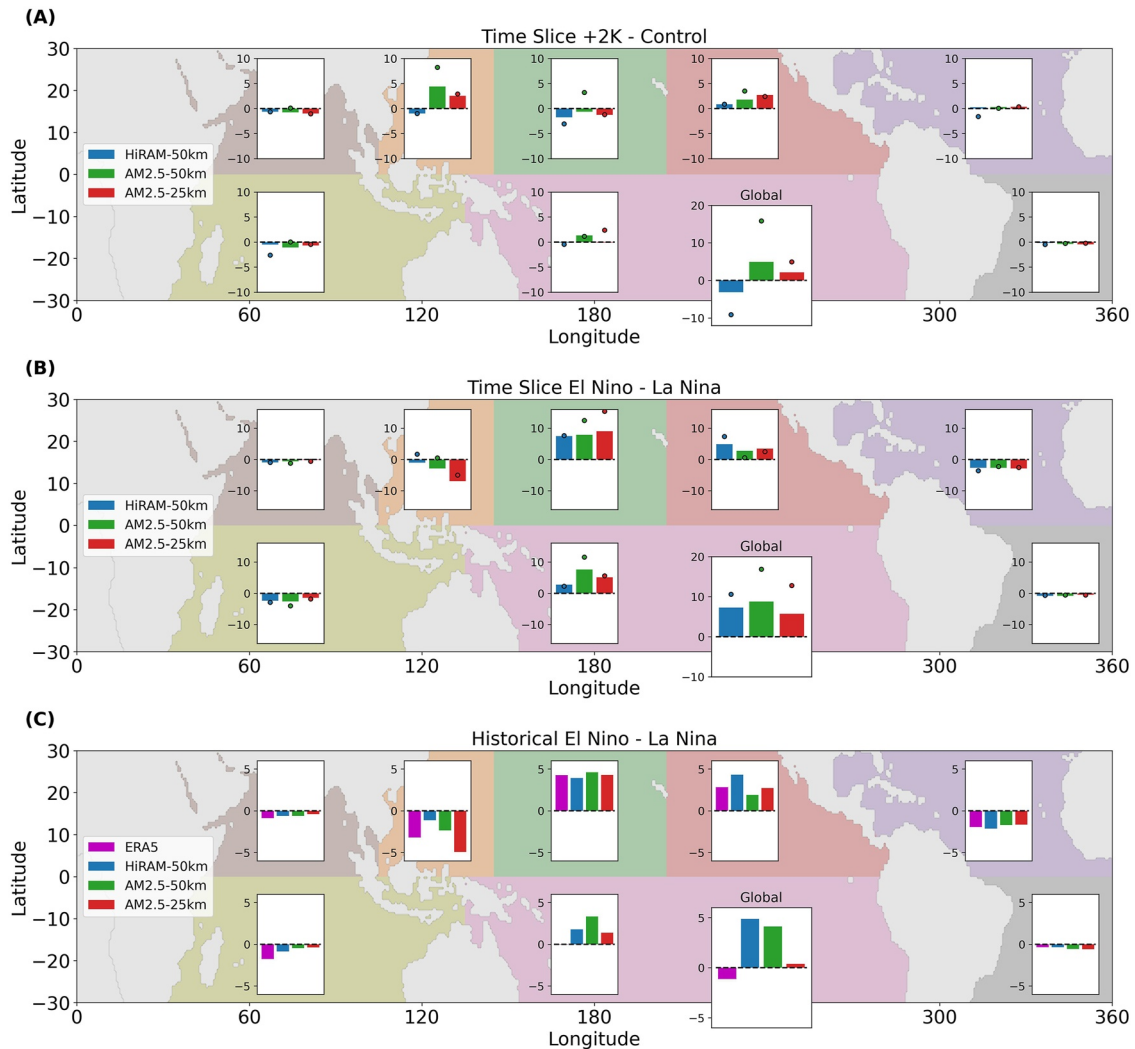


Figure 2. Maps of the seed propensity index (SPI) change. Basin-wide contributions of SPI (bars) to the global percentage change between (a) the uniform 2 K warming and the control climates, (b) the time slice (repeating annual cycle) El Niño and La Niña experiments, and (c) composites of the historical El Niño and La Niña years. The percentage change of the simulated seed frequency (circles) is shown for the time slice experiments in (a) and (b). The sum over all basins equals the global percentage change.

Figure 2a compares the seed frequency and SPI in response to uniform 2 K warming across ocean basins and models. SPI underestimates the global seed frequency because some weather-scale variability is not captured by the monthly mean, but the model spread in seed frequency follows the pattern of the model spread in SPI. The seed frequency is the most inconsistent over the Northwest and Northcentral Pacific, especially in the sign of response, and SPI qualitatively captures this model spread. HiRAM-50km shows a weakening of large-scale atmospheric ascent over the Northwest Pacific, where SPI decreases. On the other hand, the weakening does not occur in the two AM2.5 models.

In Figure 2b, the percentage change between the time slice El Niño and La Niña experiments are used to investigate a different large-scale atmospheric ascent pattern. SPI qualitatively captures the inter-basin variability and the model spread in seed frequency change between the El Niño and La Niña experiments. The models show a consistent decrease in the North Atlantic; while the Northwest Pacific is again more inconsistent across models.

The modeled SPI can also be compared with the reanalysis when sufficient number of years are averaged over. Using the historical simulations driven by the observed SST time series, years with Oceanic Niño Indices greater than 1 and less than -1 are respectively averaged over (detailed in Section 2.2). This procedure yields a composite

of the nine strongest El Niño years and a composite of the seven strongest La Niña years. The percentage change between the El Niño and La Niña composites, averaged over all ensemble members, is shown in Figure 2c. The same procedure is applied to the ERA5 (Hersbach et al., 2020) reanalyzed circulation, except no ensemble mean is taken. Seeds are not tracked in this panel as they are not well-defined in the reanalysis.

The inter-basin variability is fairly consistent across models and reanalysis. All models and the reanalysis capture the decrease of SPI in the North Atlantic and the increase of SPI in the Northeast Pacific in the El Niño years, consistent with the observed interannual variability of TC frequency (Sobel et al., 2021). In the Northwest Pacific, the inter-model distinctions are slightly larger but are insufficient data to rule out the plausibility of either model against the observed El Niño-Southern Oscillation (ENSO), despite the fact that the models have qualitatively different future projections.

4. Summary

This study presents a large number of model experiments and shows that the seed frequency strongly influences the TC frequency across climate perturbations and models having different convective parameterizations and resolutions. For the more plausible climate perturbations, including uniform warming, CO₂ doubling, RCP4.5, and El Niño/La Niña patterns, the seed response is linearly correlated with the TC response across models. For very strong but climatically implausible changes in tropical SST gradients (the two warming 28C perturbations), it is necessary to consider the effect of entropy ventilation, as is the case for the TC annual cycle (Yang et al., 2021). Even though the models are more consistent in the response to ENSO, they disagree in the response to uniform warming.

In all experiments performed here, the seed variation is explained by the climatological circulation, quantified by SPI which represents the large-scale ascent weighted by a function of the large-scale absolute vorticity. This downscaling formula is agnostic to the synoptic-scale phenomena, as long as the climatological circulation is set up by the radiative and surface forcings. This may explain why in the limited-domain simulation of Patricola et al. (2018), the atmospheric circulation in the North Atlantic generates seeds despite the African Easterly waves being artificially suppressed.

We have shown that SPI describes the propensity to generate convective weak vortices, which is a simple definition of seeds based only on the precipitation and vorticity fields. Alternatively, seeds are defined in some studies by using a weaker vorticity threshold in the TC tracking algorithm (Ikehata & Satoh, 2021; Sugi et al., 2020; Vidale et al., 2021; Yamada et al., 2021). Our definition and the alternative definition of seeds have similar spatial distributions and transition probability to TCs (Hsieh, Vecchi, et al., 2020). In general, seeds in our definition are more strongly correlated with SPI, but both definitions of seeds are correlated with TCs.

The seed propensity index provides a simplified framework in which to analyze the physical processes influencing the seed frequency. For instance, the denominator of Z is indicative of barotropic instability (Bembenek et al., 2021; Hsieh, Vecchi, et al., 2020), which may lead to the break down of the ITCZ and generate seeds; ω is determined by the large-scale energy flux convergence and the gross moist stability, which may be influenced by the cloud radiative feedback or the entrainment rate (Zhao et al., 2018) and may depend on the horizontal resolution. We have shown that the correlation between the seed frequency and SPI applies across model resolutions, but their values may co-vary with resolution. Ongoing research addresses how these physical processes influence the seed frequency and in turn the TC frequency.

Conflict of Interest

The authors declare no conflicts of interest relevant to this study.

Data Availability Statement

The model source code is available from <https://www.gfdl.noaa.gov/atmospheric-model/>. The ERA5 data set is available from <https://doi.org/10.24381/cds.6860a573>. Python scripts for tracking seeds and computing the seed propensity index are available from https://github.com/tlhsieh/tropical_cyclone_seeds and are permanently archived at <https://doi.org/10.5281/zenodo.6193045>.

Acknowledgments

We thank Zhihong Tan for comments on an earlier version of the manuscript. We thank Isaac Held and Thomas Knutson for discussion. The HiRAM-50km, AM2.5-50km and AM2.5-25km simulations were performed on computational resources managed and supported by Princeton Research Computing, a consortium of groups including the Princeton Institute for Computational Science and Engineering, the Office of Information Technology's High Performance Computing Center, and the Visualization Laboratory at Princeton University. The AM4-50km simulations were performed on the Geophysical Fluid Dynamics Laboratory High Performance Computing System. This work has been supported by National Oceanic and Atmospheric Administration (NOAA)/OCO (award NA18OAR4310418), NOAA/MAPP (award NA18OAR4310273), and the Carbon Mitigation Initiative at Princeton University.

References

- Bembek, E., Merlis, T. M., & Straub, D. N. (2021). Influence of latitude and moisture effects on the barotropic instability of an idealized ITCZ. *Journal of the Atmospheric Sciences*, 78(9), 2677–2689. <https://doi.org/10.1175/jas-d-20-0346.1>
- Bhatia, K., Vecchi, G., Murakami, H., Underwood, S., & Kossin, J. (2018). Projected response of tropical cyclone intensity and intensification in a global climate model. *Journal of Climate*, 31(20), 8281–8303. <https://doi.org/10.1175/jcli-d-17-0898.1>
- Bister, M., & Emanuel, K. A. (2002). Low frequency variability of tropical cyclone potential intensity 1. Interannual to interdecadal variability. *Journal of Geophysical Research*, 107(D24), ACL-26-1–ACL-26-15. <https://doi.org/10.1029/2001jd000776>
- Camargo, S. J., Tippett, M. K., Sobel, A. H., Vecchi, G. A., & Zhao, M. (2014). Testing the performance of tropical cyclone genesis indices in future climates using the HiRAM model. *Journal of Climate*, 27(24), 9171–9196. <https://doi.org/10.1175/jcli-d-13-00505.1>
- Chen, J.-H., & Lin, S.-J. (2011). The remarkable predictability of inter-annual variability of Atlantic hurricanes during the past decade. *Geophysical Research Letters*, 38(11), L11804. <https://doi.org/10.1029/2011gl047629>
- Durack, P. J., & Taylor, K. E. (2018). *PCMDI AMIP SST and sea-ice boundary conditions version 1.1.4*. <https://doi.org/10.22033/ESGF/input4MIPs.2204>
- Emanuel, K. (2020). Response of global tropical cyclone activity to increasing CO₂: Results from downscaling CMIP6 models. *Journal of Climate*, 34(1), 57–70.
- Gray, W. M. (1979). Hurricanes: Their formation, structure and likely role in the tropical circulation. In *Meteorology over the tropical oceans*, (pp. 155–218). Royal Meteorological Society.
- Harris, L. M., Lin, S.-J., & Tu, C. (2016). High-resolution climate simulations using GFDL HiRAM with a stretched global grid. *Journal of Climate*, 29(11), 4293–4314. <https://doi.org/10.1175/jcli-d-15-0389.1>
- Held, I. M., & Zhao, M. (2011). The response of tropical cyclone statistics to an increase in CO₂ with fixed sea surface temperatures. *Journal of Climate*, 24(20), 5353–5364. <https://doi.org/10.1175/jcli-d-11-00050.1>
- Hersbach, H., Bell, B., Berrisford, P., Hirahara, S., Horányi, A., Muñoz-Sabater, J., et al. (2020). The ERA5 global reanalysis. *Quarterly Journal of the Royal Meteorological Society*, 146(730), 1999–2049. <https://doi.org/10.1002/qj.3803>
- Hoogewind, K. A., Chavas, D. R., Schenkel, B. A., & O'Neill, M. E. (2020). Exploring controls on tropical cyclone count through the geography of environmental favorability. *Journal of Climate*, 33(5), 1725–1745. <https://doi.org/10.1175/jcli-d-18-0862.1>
- Hsieh, T.-L. (2022). *tropical_cyclone_seeds*. *Zenodo*. <https://doi.org/10.5281/ZENODO.6193044>
- Hsieh, T.-L., Garner, S. T., & Held, I. M. (2020). Hypohydrostatic simulation of a quasi-steady baroclinic cyclone. *Journal of the Atmospheric Sciences*, 77(4), 1415–1428. <https://doi.org/10.1175/jas-d-19-0300.1>
- Hsieh, T.-L., Vecchi, G. A., Yang, W., Held, I. M., & Garner, S. T. (2020). Large-scale control on the frequency of tropical cyclones and seeds: A consistent relationship across a hierarchy of global atmospheric models. *Climate Dynamics*, 55(11), 3177–3196. <https://doi.org/10.1007/s00382-020-05446-5>
- Ikehata, K., & Satoh, M. (2021). Climatology of tropical cyclone seed frequency and survival rate in tropical cyclones. *Geophysical Research Letters*, 48(18), e2021GL093626. <https://doi.org/10.1029/2021gl093626>
- Jeevanjee, N., & Romps, D. M. (2018). Mean precipitation change from a deepening troposphere. *Proceedings of the National Academy of Sciences*, 115(45), 11465–11470. <https://doi.org/10.1073/pnas.1720683115>
- Jing, R., Lin, N., Emanuel, K., Vecchi, G., & Knutson, T. R. (2021). A comparison of tropical cyclone projections in a high-resolution global climate model and from downscaling by statistical and statistical-deterministic methods. *Journal of Climate*, 34(23), 9349–9364. <https://doi.org/10.1175/jcli-d-21-0071.1>
- Knutson, T., Camargo, S. J., Chan, J. C. L., Emanuel, K., Ho, C.-H., Kossin, J., et al. (2020). Tropical cyclones and climate change assessment: Part II: Projected response to anthropogenic warming. *Bulletin of the American Meteorological Society*, 101(3), E303–E322. <https://doi.org/10.1175/bams-d-18-0194.1>
- Lee, C.-Y., Camargo, S. J., Sobel, A. H., & Tippett, M. K. (2020). Statistical-dynamical downscaling projections of tropical cyclone activity in a warming climate: Two diverging genesis scenarios. *Journal of Climate*, 33(11), 4815–4834. <https://doi.org/10.1175/jcli-d-19-0452.1>
- Murakami, H., Vecchi, G. A., Underwood, S., Delworth, T. L., Wittenberg, A. T., Anderson, W. G., et al. (2015). Simulation and prediction of category 4 and 5 hurricanes in the high-resolution GFDL HiFLOR coupled climate model. *Journal of Climate*, 28(23), 9058–9079. <https://doi.org/10.1175/jcli-d-15-0216.1>
- Patricola, C. M., Saravanan, R., & Chang, P. (2018). The response of Atlantic tropical cyclones to suppression of African Easterly waves. *Geophysical Research Letters*, 45(1), 471–479. <https://doi.org/10.1002/2017gl076081>
- Roberts, M. J., Camp, J., Seddon, J., Vidale, P. L., Hodges, K., Vannièrè, B., et al. (2020). Projected future changes in tropical cyclones using the CMIP6 HighResMIP multimodel ensemble. *Geophysical Research Letters*, 47(14), e2020GL088662. <https://doi.org/10.1029/2020gl088662>
- Sobel, A. H., Wing, A. A., Camargo, S. J., Patricola, C. M., Vecchi, G. A., Lee, C.-Y., & Tippett, M. K. (2021). Tropical cyclone frequency. *Earth's Future*, 9(12), e2021EF002275. <https://doi.org/10.1029/2021ef002275>
- Sugi, M., Yamada, Y., Yoshida, K., Mizuta, R., Nakano, M., Kodama, C., & Satoh, M. (2020). *Future changes in the global frequency of tropical cyclone seeds*. advpub.
- Tang, B., & Camargo, S. J. (2014). Environmental control of tropical cyclones in CMIP5: A ventilation perspective. *Journal of Advances in Modeling Earth Systems*, 6(1), 115–128. <https://doi.org/10.1002/2013ms000294>
- Tang, B., & Emanuel, K. (2012). A ventilation index for tropical cyclones. *Bulletin of the American Meteorological Society*, 93(12), 1901–1912. <https://doi.org/10.1175/bams-d-11-00165.1>
- van der Wiel, K., Kapnick, S. B., & Vecchi, G. A. (2017). Shifting patterns of mild weather in response to projected radiative forcing. *Climatic Change*, 140(3), 649–658. <https://doi.org/10.1007/s10584-016-1885-9>
- Vecchi, G. A., Delworth, T., Gudgel, R., Kapnick, S., Rosati, A., Wittenberg, A. T., et al. (2014). On the seasonal forecasting of regional tropical cyclone activity. *Journal of Climate*, 27(21), 7994–8016. <https://doi.org/10.1175/jcli-d-14-00158.1>

- Vecchi, G. A., Delworth, T. L., Murakami, H., Underwood, S. D., Wittenberg, A. T., Zeng, F., et al. (2019). Tropical cyclone sensitivities to CO₂ doubling: Roles of atmospheric resolution, synoptic variability and background climate changes. *Climate Dynamics*, *53*(9), 5999–6033. <https://doi.org/10.1007/s00382-019-04913-y>
- Vidale, P. L., Hodges, K., Vanni re, B., Davini, P., Roberts, M. J., Strommen, K., et al. (2021). Impact of stochastic Physics and model resolution on the simulation of tropical cyclones in climate GCMs. *Journal of Climate*, *34*(11), 4315–4341. <https://doi.org/10.1175/jcli-d-20-0507.1>
- Walsh, K. J. E., Camargo, S. J., Vecchi, G. A., Daloz, A. S., Elsner, J., Emanuel, K., et al. (2015). Hurricanes and climate: The U.S. CLIVAR working group on hurricanes. *Bulletin of the American Meteorological Society*, *96*(6), 997–1017. <https://doi.org/10.1175/bams-d-13-00242.1>
- Yamada, Y., Kodama, C., Satoh, M., Sugi, M., Roberts, M. J., Mizuta, R., et al. (2021). Evaluation of the contribution of tropical cyclone seeds to changes in tropical cyclone frequency due to global warming in high-resolution multi-model ensemble simulations. *Progress in Earth and Planetary Science*, *8*(1), 11. <https://doi.org/10.1186/s40645-020-00397-1>
- Yang, W., Hsieh, T.-L., & Vecchi, G. A. (2021). Hurricane annual cycle controlled by both seeds and genesis probability. *Proceedings of the National Academy of Sciences*, *118*(41), e2108397118. <https://doi.org/10.1073/pnas.2108397118>
- Zhao, M. (2020). Simulations of atmospheric rivers, their variability, and response to global warming using GFDL’s new high-resolution general circulation model. *Journal of Climate*, *33*(23), 10287–10303. <https://doi.org/10.1175/jcli-d-20-0241.1>
- Zhao, M., Golaz, J.-C., Held, I. M., Guo, H., Balaji, V., Benson, R., et al. (2018). The GFDL global atmosphere and land model AM4.0/LM4.0: 1. Simulation characteristics with prescribed SSTs. *Journal of Advances in Modeling Earth Systems*, *10*(3), 691–734. <https://doi.org/10.1002/2017ms001208>
- Zhao, M., & Held, I. M. (2010). An analysis of the effect of global warming on the intensity of Atlantic hurricanes using a GCM with statistical refinement. *Journal of Climate*, *23*(23), 6382–6393. <https://doi.org/10.1175/2010jcli3837.1>
- Zhao, M., Held, I. M., Lin, S.-J., & Vecchi, G. A. (2009). Simulations of global hurricane climatology, interannual variability, and response to global warming using a 50 km resolution GCM. *Journal of Climate*, *22*(24), 6653–6678. <https://doi.org/10.1175/2009jcli3049.1>